nature structural & molecular biology

Clathrin-coat disassembly illuminates the mechanisms of Hsp70 force generation

Rui Sousa[1], Hsien-Shun Liao[2,4], Jorge Cuéllar[3], Suping Jin[1], José M Valpuesta[3], Albert J Jin[2] & Eileen M Lafer[1]

Hsp70s use ATP hydrolysis to disrupt protein-protein associations and to move macromolecules. One example is the Hsc70-mediated disassembly of the clathrin coats that form on vesicles during endocytosis. Here, we exploited the exceptional features of these coats to test three models—Brownian ratchet, power-stroke and entropic pulling—proposed to explain how Hsp70s transform their substrates. Our data rule out the ratchet and power-stroke models and instead support a collision-pressure mechanism whereby collisions between clathrin-coat walls and Hsc70s drive coats apart. Collision pressure is the complement to the pulling force described in the entropic pulling model. We also found that self-association augments collision pressure, thereby allowing disassembly of clathrin lattices that have been predicted to be resistant to disassembly. These results illuminate how Hsp70s generate the forces that transform their substrates.

Hsp70s inhibit the formation of nonfunctional protein complexes and aggregates by sequestering interactive (primarily hydrophobic) segments of both native and misfolded protein substrates[1,2]. The conformational changes that allow Hsp70s to alternately bind and release their substrates are understood[3–7] but do not explain how Hsp70s disassociate aggregates or complexes[8–11], or pull proteins into organelles[12,13]. In these reactions, Hsp70s move their substrates, either through translocation pores or away from other proteins. Under the power-stroke model, Hsp70, during ATP hydrolysis, undergoes a conformational change that pulls on its substrate[12]. Under the Brownian ratchet model, Hsp70 asymmetrically traps spontaneous fluctuations that move the substrate in a particular direction[14,15]. Finally, under the entropic pulling model[16,17], Hsp70 recruitment to its substrate results in an Hsp70 bound to a floppy polypeptide abutting a structural wall (for example, an aggregate or translocation pore). Movement of Hsp70 away from the wall, dragging the polypeptide substrate with it, is thermodynamically favored because it increases Hsp70's freedom of motion and entropy.

Clathrin uncoating, in which constitutively expressed Hsc70 is recruited to coated vesicles by the J cochaperone auxilin and then drives coat disassembly into triskelia (trimers of clathrin heavy- and light-chain dimers)[2], provides an exceptional system through which to study how Hsp70s alter their substrates. Clathrin-cage assembly and disassembly *in vitro*[18] can be precisely monitored in both single-molecule[19,20] and ensemble experiments[21]. Cage stability can be modulated by pH[22]. Structures of cages and other reaction components have been reported[3,23–26], and a single Hsc70-binding site at the clathrin heavy-chain (CHC) C terminus mediates disassembly[27].

We set out to test models of Hsp70 force generation by exploiting these features. Our results do not support the power-stroke or Brownian-ratchet models but instead support the entropic pulling model. They also show that Hsp70 oligomerization, a ubiquitous phenomenon with no known active biological function[28–30], augments the force that Hsp70s generate when acting on their substrates.

RESULTS

The three models in the context of uncoating

Clathrin-cage disassembly is driven by Hsc70 binding to a sequence (QLMLT) in the flexible CHC C-terminal tail ten residues downstream of each of the three helices at the center of the triskelion under each cage vertex[23,27] (**Fig. 1a**,**b**). In previous structural studies, it has been proposed that Hsc70 does not induce but instead sterically locks in fluctuations that loosen the clathrin lattice until they accumulate to a point that disassembly ensues[23]. This Brownian/steric-wedge model can be tested by moving the Hsc70-binding site to relieve steric clashes between the Hsc70 and cage walls. If disassembly were to persist even as steric clashes are relieved, this mechanism would be less plausible.

The entropic pulling model emphasizes thermodynamics—the entropy change—in the reaction[16,17], but the complementary molecular kinetic description is collision pressure, in which collisions and repulsion between Hsp70s and closely apposed structural walls impart momentum away from the walls[31,32] and to the Hsp70s. Such collisions necessarily generate equal and opposite momentum on the walls. Thus, Hsc70s bound to flexible tethers under each vertex would impart pressure against cage walls and consequently drive the triskelia apart. In contrast to the steric-wedge model, the collision-pressure

[1]Department of Biochemistry and Center for Biomedical Neuroscience, University of Texas Health Science Center at San Antonio, San Antonio, Texas, USA. [2]Laboratory of Cellular Imaging and Macromolecular Biophysics, National Institute of Biomedical Imaging and Bioengineering, National Institutes of Health, Bethesda, Maryland, USA. [3]Department for Macromolecular Structures, Centro Nacional de Biotecnología (CNB-CSIC), Madrid, Spain. [4]Present address: Department of Mechanical Engineering, National Taiwan University, Taipei, Taiwan. Correspondence should be addressed to R.S. (sousa@uthscsa.edu).

Received 1 March; accepted 6 July; published online 1 August 2016; doi:10.1038/nsmb.3272

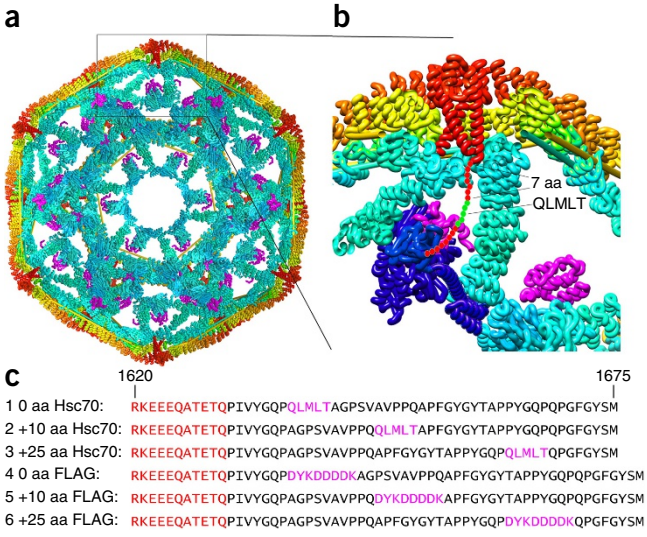

Figure 1 Structural context of approaches to test Hsc70 disassembly mechanisms. (**a**) Cut-away view of the clathrin cage (interior surface in cyan; exterior in yellow and orange) with auxilin (magenta; PDB 1XI5 (ref. 23)). C termini of CHCs form a helical tripod (red) under each vertex. (**b**) Expanded view of the boxed region in **a**. Hsc70 (PDB 4B9Q[3]; blue) modeled into the clathrin–auxilin cage on the basis of an Hsp70 NBD–auxilin J-domain structure[26], in which the protein-binding domain (PBD) is positioned to bind the terminal tail (shown as red circles with the Hsc70-binding QLMLT sequence in green). (**c**) Sequences of the termini of the CHCs used (sequence 1 is WT), with helical segments in red and Hsc70-binding and FLAG sites in magenta.

mechanism suggests that moving the Hsc70-binding site away from the walls would slow but not stop disassembly and that moving this site by 10 or 25 amino acids (aa) would slow disassembly by ~10- or ~60-fold, respectively[17] (**Supplementary Note 1**).

The collision-pressure and Brownian/steric-wedge models predict that any protein similar in size to Hsc70 and binding at the same location should drive disassembly, whereas the power-stroke model requires an Hsc70-specific conformational change. Therefore, in contrast to the steric wedge and collision-pressure models, the power-stroke mechanism suggests that if the Hsc70-binding site were replaced with an antibody-binding site, the antibody should not drive disassembly.

To test the mutually exclusive predictions of these models, we assembled cages from CHCs in which the Hsc70-binding site was at its wild-type (WT) position (0 aa), or 10 or 25 aa C-terminal to this position (+10 aa and +25 aa; **Fig. 1c**). We also prepared cages with this site replaced with an antibody-binding site (a FLAG tag) at the WT position, or 10 or 25 aa C-terminal to this position (denoted 0-aa FLAG, +10-aa FLAG and +25-aa FLAG; **Fig. 1c**).

Moving the Hsc70-binding site slows disassembly

We measured disassembly on the basis of light-scattering in a stopped-flow fluorometer (**Supplementary Fig. 1**), using cages reacted with varying concentrations of Hsc70. With 0-aa cages, reaction profiles (**Fig. 2a**) were similar to those seen by Rothnie *et al.*, who have used a similar approach[21]. The reaction of cages with 2 μM Hsc70 resulted in an initial ~15% increase in scattering, which was followed by a drop to ~20% of the initial level. The large drop was due to disassembly[21,24]. The nature of the initial smaller increase is unknown but was assigned by Rothnie *et al.* to the binding of the first Hsc70 to one of the three CHC termini in their sequential mechanism, in which three Hsc70s must bind all three sites in a triskelion before that triskelion is released from the cage. A subsequent single-molecule study has cast doubt over this mechanism by showing that disassembly begins when only one or even fewer[20] Hsc70s are bound for every two triskelia, and that Hsc70s continue to bind and accelerate disassembly even after disassembly had begun[19].

We attempted to fit our data by using the sequential scheme described Rothnie *et al.* but concluded that neither the amplitude of the initial increase in scattering nor the rates of this initial increase or subsequent decrease could be accurately determined, because these parameters are coupled (**Supplementary Fig. 2**). We therefore used the simplest possible scheme: C + H → CH → T, where C, H and T correspond to cages, Hsc70 and triskelia, respectively (**Supplementary Note 2**) to fit values for the rate of Hsc70 association (k_a), the amplitude of scattering from the intermediate (CH) and the cage-disassembly rate (k_d). However, because these parameters are coupled, we did not ascribe meaning to these values but instead derived a parameter that was independent of the amplitude of the intermediate and incorporated both the association and disassembly rates: $k_{ov} = 1/(1/([\text{Hsc70}] \times k_a)+1/k_d))$, in which square brackets denote concentration. This equation corresponds to the overall rate of disassembly ($k_3^+ = 0.105\ \mu M^{-1}\ s^{-1}$) described by Bocking *et al.*[19]. Bocking *et al.* have concluded that this rate increases linearly with Hsc70 concentration. However, this conclusion is inconsistent with their data, which show large divergence from linearity at Hsc70 concentrations > 1 μM (ref. 19), and also with our data (**Fig. 2d–f**) and those from Rothnie *et al.*[21], which show hyperbolic kinetics. We therefore fitted overall rates at different Hsc70 concentrations to a hyperbolic equation (**Fig. 2d**). With 0-aa cages, we obtained a V_{max} of 0.11 s^{-1} with an $[\text{Hsc70}]_{1/2Vmax}$ of 0.34 μM, and a rate of 0.065 s^{-1} at 0.5 μM Hsc70, a result similar to the estimate of 0.053 s^{-1} with 0.5 μM Hsc70 (a concentration at which divergence from their linear model was small) in Bocking *et al.*

With +10-aa and +25-aa cages, disassembly was, respectively, two- and four-fold slower than with 0 aa cages (**Fig. 2**). Disassembly of cages missing the Hsc70-binding site was ~20× slower (**Supplementary Fig. 1**), thus indicating that disassembly of +10-aa or +25-aa cages was predominately due to Hsc70 binding to the displaced site. The initial scattering increase became larger as the Hsc70-binding site was moved, reaching ~70% of the starting value in reactions with +25-aa cages (**Fig. 2c**).

Our observation that disassembly slowed by only four-fold even when the Hsc70-binding site was moved 25 aa does not support the Brownian/steric-wedge model but is also inconsistent with the collision-pressure model, which predicts an ~60-fold decrease when the binding site is moved to this extent. We wondered whether this result might be due to Hsc70 self-association[28], because the collision-pressure model assumes identical numbers of Hsc70s binding to cages with different tether lengths. We tested this possibility with Hsc70ΔC, which is functional in disassembly but bears a C-terminal deletion that decreases self-association[33]. With Hsc70ΔC and 0-aa cages, the maximal disassembly rate was approximately two-fold slower, and the $1/2V_{max}$ concentration was approximately two-fold greater than that with Hsc70 (**Fig. 2g**). However, with +10-aa and +25-aa cages, disassembly with Hsc70ΔC was much slower than with Hsc70 (**Fig. 2h,i**), and we were not able to determine V_{max} because the rates did not plateau over the tested concentration range. Instead, we compared rates at 2 μM Hsc70ΔC and obtained values of 0.051 s^{-1}, 0.0078 s^{-1} and 0.00080s^{-1} for the 0-aa, +10-aa and +25-aa cages, respectively (**Fig. 2g–i** and **Supplementary Table 1**). Thus, with Hsc70ΔC, the rate decreases were in agreement with the collision-pressure model. With Hsc70ΔC, the initial scattering increase was also smaller than that with Hsc70, reaching a maximum of ~40% (with +25-aa cages; **Fig. 2i**) but reaching ~70% with Hsc70 (**Fig. 2c**).

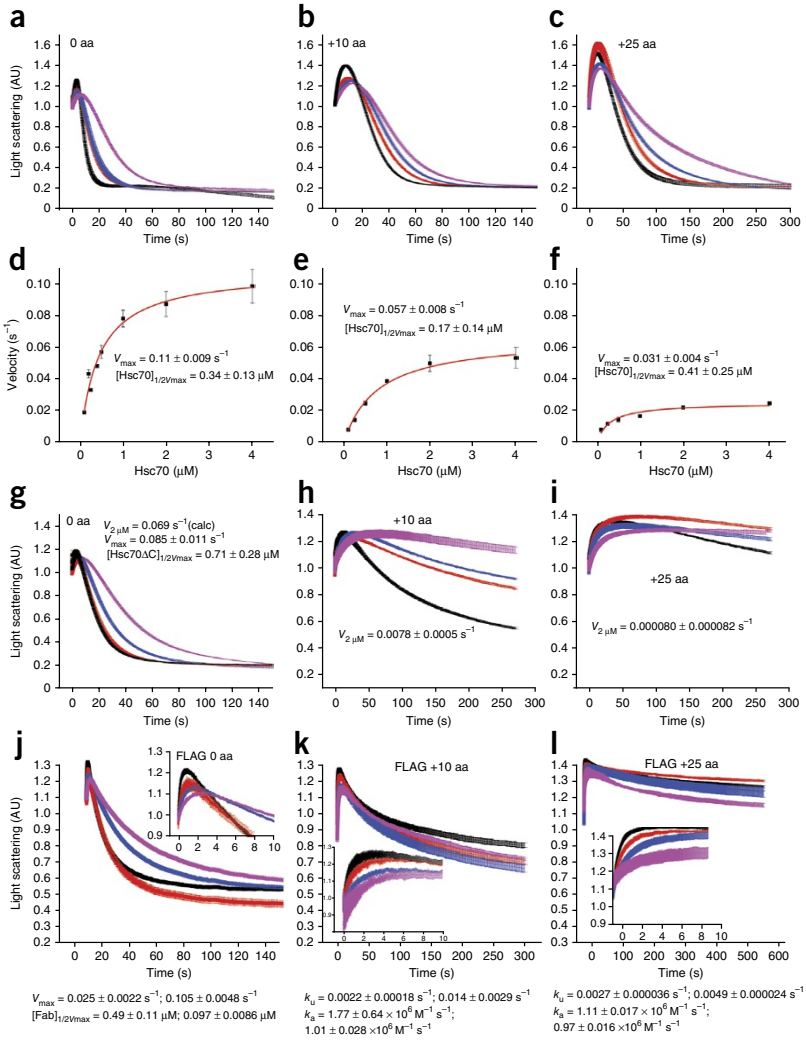

Figure 2 Moving the Hsc70-binding site slows disassembly and reveals a reaction intermediate of large scattering amplitude, and replacing it with a FLAG tag allows disassembly by anti-FLAG Fabs. (**a**) Scattering (normalized to a starting value of 1) versus time for reactions with WT (0 aa) cages reacted with 0.25 (magenta), 0.5 (blue), 1.0 (red) or 2.0 (black) μM Hsc70. AU, arbitrary units. (**b**) As in **a**, but with the Hsc70-binding site moved 10 aa downstream (+10 aa). (**c**) As in **a**, but with the Hsc70-binding site moved 25 aa (+25 aa). (**d**) Hyperbolic fits of WT cage disassembly rates versus Hsc70 concentration. (**e**) As in **d**, but for +10-aa cages. (**f**) As in **d**, but for +25-aa cages. (**g**) As in **a**, but with Hsc70ΔC. (**h**) As in **g**, but with +10-aa cages. (**i**) As in **g**, but with +25-aa cages. (**j**) As in **a**, but with anti-FLAG Fab and cages with the Hsc70-binding site replaced with a FLAG tag. (**k**) As in **j**, but with the tag shifted 10 aa. (**l**) As in **j**, but with the tag moved 25 aa. In **j**–**l**, insets show the initial 10 s of reactions to resolve the Fab binding phase. For all plots, trace thickness, error bars and fitted values indicate ± s.e.m. The number of replicates for each experimental condition is specified in **Supplementary Table 3**. Source data for the graphs are available online.

Anti-FLAG Fabs disassemble FLAG-tag cages

To test the power-stroke model, we evaluated the ability of anti-FLAG Fab to disassemble FLAG-tag cages. We used Fab (50 kDa) rather than IgG because Fab is similar in molecular weight to Hsc70 (70 kDa) or Hsc70ΔC (60 kDa) and because divalent binding may cross-link CHCs and inhibit disassembly (**Supplementary Fig. 3**). When the tag was at the same position as the WT Hsc70-binding site, Fab disassembled cages at rates similar to those of Hsc70 or Hsc70ΔC (**Fig. 2j**). However, when the tag was moved 10 or 25 aa downstream (**Fig. 2k.l**), the rates slowed approximately 8- or 40-fold, respectively, similarly to our observations for Hsc70ΔC and in agreement with the collision-pressure model. The amplitude of the initial increase in scattering with Fab was also similar to that observed with Hsc70ΔC. However, the rate of this increase was faster, reaching completion within 1–2 s with Fab but extending over 5–25 s with Hsc70ΔC. This result probably reflects that Hsc70 must first bind ATP and then auxilin, and is then transferred to clathrin in a step limited by an ATP-hydrolysis rate of ~0.1 s^{-1} (ref. 34). The rate of the initial increase with Fab indicates a binding rate of 1 × 10^6 to 2 × 10^6 M^{-1} s^{-1}, values consistent with known antibody binding rates[35].

Hsc70 markedly increases scattering by low-pH-stabilized cages

As the Hsc70-binding site was shifted, disassembly slowed, and the initial scattering increase became larger (**Fig. 2a–c**). We propose that this occurs because when disassembly is fast, the potential amplitude of this increase is obscured because, before reaching its maximum, scattering drops as disassembly ensues. However, kinetic coupling (**Supplementary Fig. 2**) precludes estimation of its maximum amplitude by fitting rate data. To measure this amplitude, we carried out reactions at pH 6.0, at which cages resist disassembly[23]. With Hsc70, we observed an ATP- and auxilin-dependent increase in scattering of ~200% of the starting value (**Fig. 3a–c**). With Fab (**Fig. 3d–f**) or Hsc70ΔC (**Fig. 3g,h**) the maximal increase was only ~50% and ~70%, respectively.

Light-scattering by a protein is a function of its dimensions and mass. To determine whether the initial increases in scattering were due to increases in cage mass, we adapted a hollow-sphere model developed to analyze scattering from vesicles[36]. For Hsc70ΔC and Fab, this model accurately predicted the amplitude of the scattering increases to be ~70% and ~55%, respectively, assuming that each of these proteins binds 1:1 to their binding sites in a cage (**Fig. 3i**). However, the model predicts a scattering increase of only ~80% for binding of Hsc70 at the same stoichiometry, thus suggesting that Hsc70 induces a larger increase in cage dimensions than does Hsc70ΔC or Fab; that a larger number of Hsc70s bind; or that Hsc70 causes cages to aggregate. We ruled out the last possibility because we saw no change in either the rate or amplitude of the Hsc70-driven scattering increase in experiments in which the cage concentration was varied (**Supplementary Fig. 4**).

Scattering increases are not due to increases in cage size

If only one Hsc70 were to bind the single Hsc70 site in each CHC, cage diameters would have to increase ~30% to explain the three-fold increase in scattering observed in reactions at pH 6 with Hsc70 (**Fig. 3a–c**). However, Xing *et al.*[23] have observed that Hsc70ΔC binding decreases cage dimensions by 0.8% along one axis and

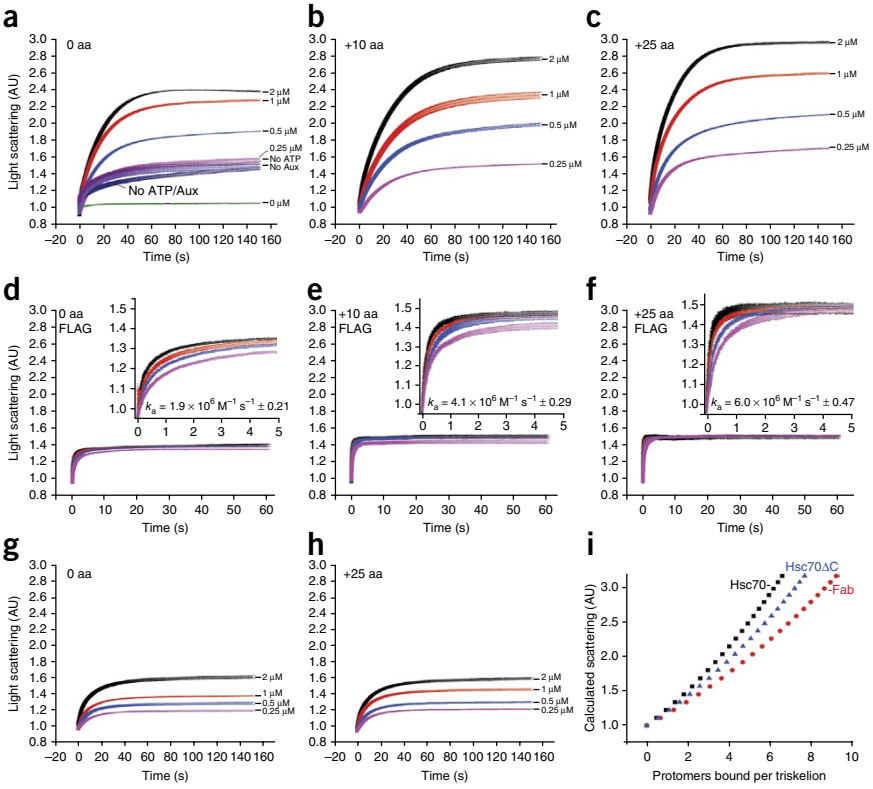

Figure 3 Hsc70 binding to cages under conditions that block disassembly leads to a massive increase in light-scattering. (**a**) Reaction of Hsc70 with cages at pH 6.0; other conditions are as in **Figure 2a**. AU, arbitrary units. Also plotted are reactions without Hsc70 (green), with 2 μM Hsc70 but no ATP (purple), without auxilin (Aux; indigo) or without ATP and auxilin (dark blue). (**b**) As in **a**, but with +10-aa cages. (**c**) As in **a**, but with +25-aa cages. (**d**) As in **a**, but with FLAG cages and Fab (inset shows first 5 s of reaction). (**e**) As in **d**, but with the tag moved 10 aa. (**f**) As in **d**, but with the tag moved 25 aa. (**g**) As in **a**, but with Hsc70ΔC. (**h**) As in **g**, but with +25-aa cages. (**i**) Calculated scattering of 70-nm-diameter cages bound by the indicated number of protomers per triskelion of Hsc70 (black squares), Hsc70ΔC (blue triangles) or Fab (red circles). The number of replicates for each experimental condition is specified in **Supplementary Table 3**. Source data for the graphs are available online. For all plots, trace thickness, error bars and fitted values indicate ± s.e.m.

increases them by 1.4% along the other two axes. Because Hsc70 might drive larger changes in size than Hsc70ΔC, we performed cryo-EM reconstructions of pH-6.0 cages with or without Hsc70 or Hsc70ΔC[23]. Our reconstructions and difference maps were similar to those published previously[23] (**Fig. 4a**,**b**), and the density due to Hsc70ΔC was attributable to envelopes of similar volume under each cage vertex. With the isosurface representation contoured at 2.5σ, a common value used for highly symmetric structures, this envelope could accommodate only a single ~25-kDa protein-binding domain (PBD) (**Fig. 4d**–**f**), thus suggesting that much of the Hsc70ΔC density was averaged out as a result of dynamic or static disorder. Cages with Hsc70 were similar in size to cages alone or with Hsc70ΔC (**Fig. 4a**–**c**), a result indicating that size changes cannot explain the large scattering increases observed when Hsc70 binds. Difference maps between cages with and without Hsc70 revealed an element positioned similarly to the density ascribed to Hsc70ΔC in the Hsc70ΔC cages (**Fig. 4f**).

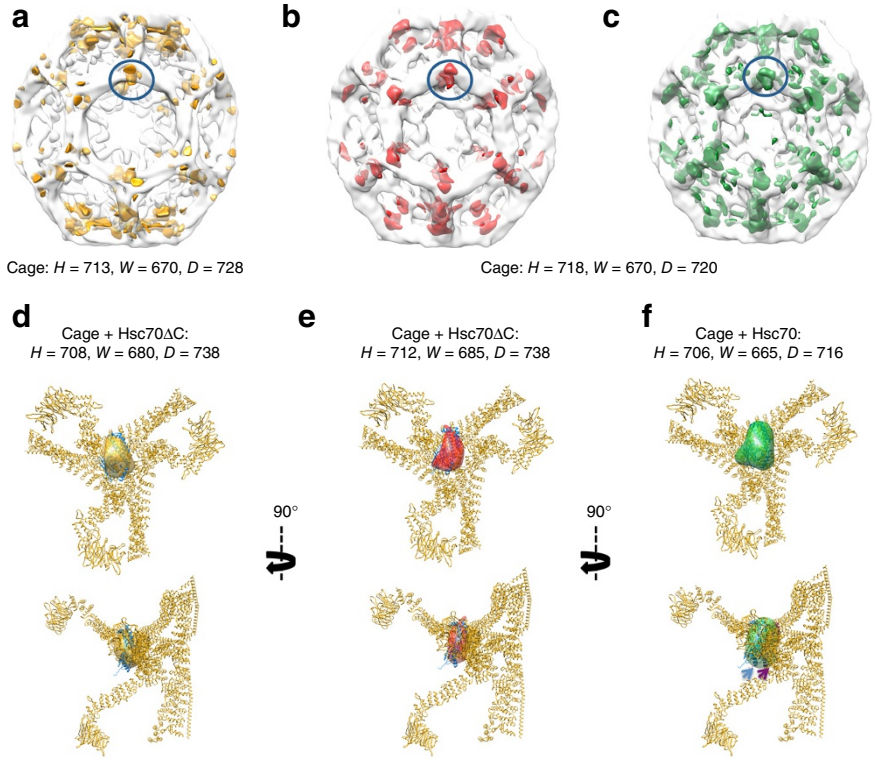

Figure 4 Cryo-EM reconstructions of cages with or without Hsc70ΔC or Hsc70. (**a**) Partially transparent cage image previously reconstructed by Xing *et al.*[23], with difference density attributable to Hsc70ΔC ((Cages + Hsc70ΔC) – (Cages)) in gold. (**b**) Partially transparent cage image from our reconstructions, with difference density attributable to Hsc70ΔC in red. (**c**) Partially transparent cage image from our reconstructions, with difference density attributable to Hsc70 in green. In each image, the bulk of the difference density is centered under each cage vertex and highlighted with blue circles. Cage dimensions ± Hsc70ΔC or Hsc70 (± 40 Å) are specified under each image. (**d**–**f**) Two orthogonal views of the ribbon model of the asymmetric unit of the clathrin cage (PDB 1XI4 (ref. 23)), with the difference density attributable to Hsc70ΔC from previous reconstructions (**d**; gold), our reconstruction with Hsc70ΔC (**e**; red) or our reconstructions with Hsc70 (**f**; green) shown. The view is from inside the cage centered on a vertex. The Hsc70ΔC density is similarly sized and positioned in both our reconstruction and the previous one, and it can accommodate one 25-kDa Hsc70 PBD (docked in the volume; PDB 1DKX[48]). The Hsc70 density is similarly positioned but is approximately twice as large and is able to accommodate two 25-kDa PBDs (indicated by blue and magenta arrows).

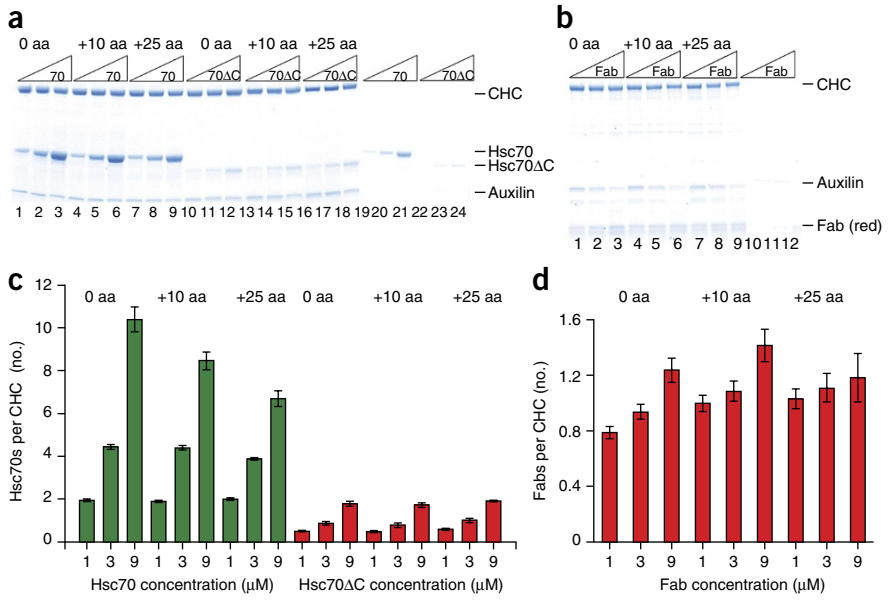

Figure 5 Scattering increases due to Hsc70 binding reflect binding of multiple Hsc70s per CHC, not cage expansion. (**a**) SDS–PAGE of pellets of the indicated cages incubated with 1, 3 or 9 μM Hsc70 (lanes 1–9) or Hsc70ΔC (lanes 10–18; Hsc70 and Hsc70ΔC concentrations increase from left to right, as indicated). Lanes 19–24 show experiments without cages. (**b**) As in **a**, but with FLAG cages and Fab (lanes 10–12 are no-cage controls). (**c**) Hsc70/CHC or Hsc70ΔC/CHC ratios plotted versus Hsc70 or Hsc70ΔC concentration, as indicated. (**d**) As in **c**, but with FLAG cages and Fab. The number of replicates for each experimental condition is specified in **Supplementary Table 3**. Source data for the graphs are available online. For all plots, trace thickness, error bars and fitted values indicate ± s.e.m.

However, although Hsc70 is only ~16% larger than Hsc70ΔC, this density was more than two-fold larger with Hsc70 than with Hsc70ΔC, thus suggesting either reduced disorder or binding of a larger number of molecules with Hsc70 than with Hsc70ΔC.

Multiple Hsc70s bind each CHC in low-pH-stabilized cages

Because cage expansion, aggregation or binding of one Hsc70 to each CHC in a cage was unable to explain the Hsc70-induced scattering increases at pH 6, we determined whether multiple Hsc70s might be binding each CHC by reacting Hsc70, Hsc70ΔC or Fab with cages at pH 6 and then pelleting the cages and their associated proteins (**Fig. 5a**,**b**). In agreement with the observed scattering and our model predictions (**Fig. 3i**), approximately one Fab per CHC bound to cages at all concentrations tested (**Fig. 5d**), whereas ~0.5, ~0.8 and ~2 Hsc70ΔCs were bound at 1, 3, and 9 μM, respectively (**Fig. 5c**). However, Hsc70 was bound in molar excess of CHC, with ~10 Hsc70s per CHC at 9 μM Hsc70 (**Fig. 5c**). Binding of such a large number of Hsc70s was dependent on auxilin, ATP and, critically, the presence of an Hsc70-binding site in the CHC (**Supplementary Fig. 5**). We conclude that the large scattering increases observed when Hsc70 was reacted with pH-6.0 cages reflect multiple Hsc70s binding per CHC, probably as a result of Hsc70 self-association, because we did not observe the same results for Hsc70ΔC.

Hsc70 self-association augments its disassembly force

The collision-pressure mechanism predicts that decreasing the number of cage-bound Hsc70s would reduce the net force that they generate against cage walls and slow the rate of disassembly. To test this possibility, we used Hsp110, a nucleotide-exchange factor (NEF) for Hsp70 (ref. 37). Hsp110 accelerates disassembly

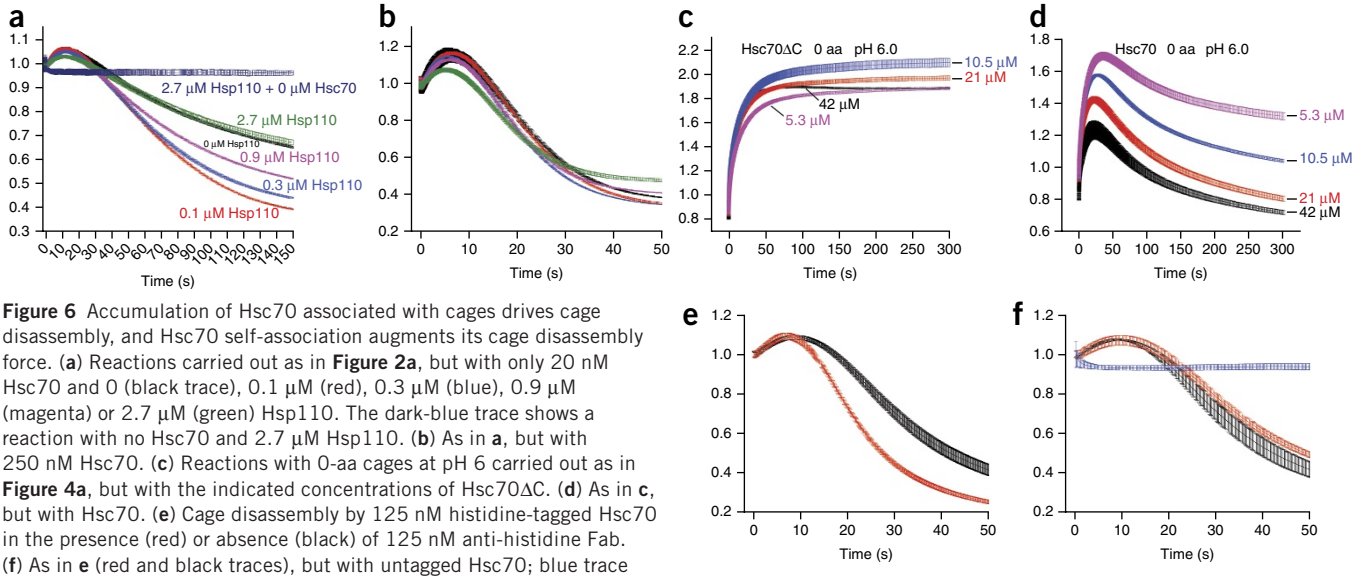

Figure 6 Accumulation of Hsc70 associated with cages drives cage disassembly, and Hsc70 self-association augments its cage disassembly force. (**a**) Reactions carried out as in **Figure 2a**, but with only 20 nM Hsc70 and 0 (black trace), 0.1 μM (red), 0.3 μM (blue), 0.9 μM (magenta) or 2.7 μM (green) Hsp110. The dark-blue trace shows a reaction with no Hsc70 and 2.7 μM Hsp110. (**b**) As in **a**, but with 250 nM Hsc70. (**c**) Reactions with 0-aa cages at pH 6 carried out as in **Figure 4a**, but with the indicated concentrations of Hsc70ΔC. (**d**) As in **c**, but with Hsc70. (**e**) Cage disassembly by 125 nM histidine-tagged Hsc70 in the presence (red) or absence (black) of 125 nM anti-histidine Fab. (**f**) As in **e** (red and black traces), but with untagged Hsc70; blue trace shows reaction of cages with anti-histidine Fab and no Hsc70. Experiments in **e** and **f** used recombinant GST-auxilin (with GST cleaved after purification) and clathrin purified from bovine brain clathrin-coated vesicles rather than recombinant histidine-tagged auxilin and CHC, to eliminate complications due to Fab binding to auxilin or CHC. The number of replicates for each experimental condition is specified in **Supplementary Table 3**. Source data for the graphs are available online. For all plots, trace thickness, error bars and fitted values indicate ± s.e.m.

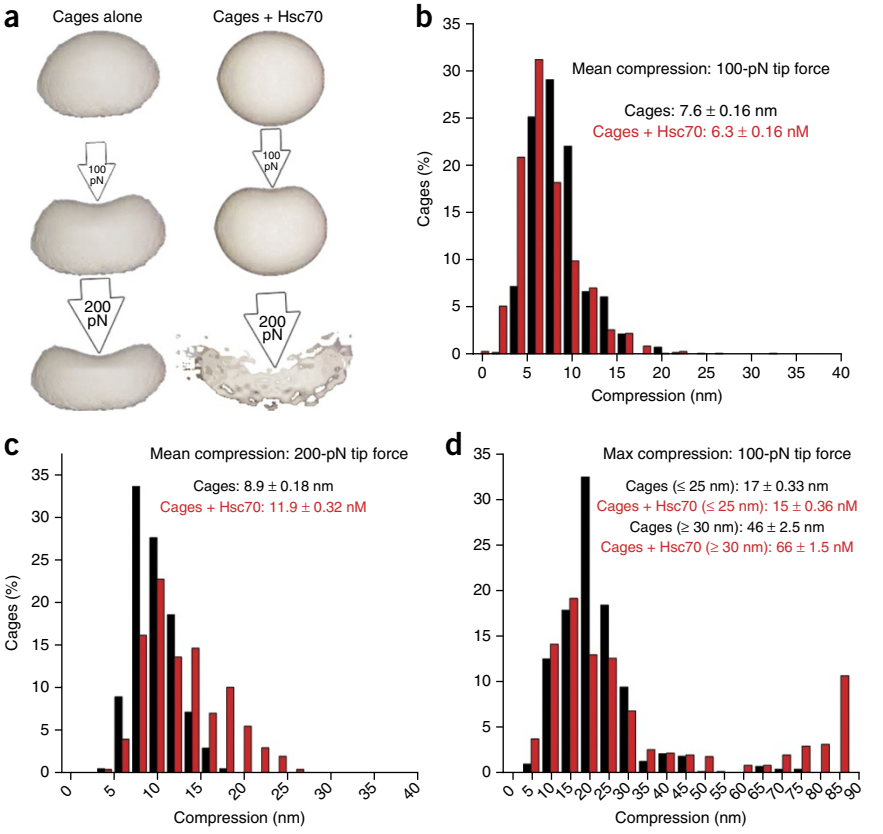

Figure 7 Hsc70 binding makes cages less compressible but more prone to catastrophic deformations. (**a**) Collision-pressure model analogizes cages either alone or with Hsc70 to balloons inflated to low and high pressure, respectively. Internal pressure generated by Hsc70s makes cages less deformable but more prone to catastrophic deformation (bursting) especially as the probing force is increased. (**b**) Percentages of cages with or without Hsc70 exhibiting the indicated mean compressions with 100-pN force. (The mean compression for each cage was determined from 9–12 measurements obtained from probing each cage on a 3 × 3 or 4 × 4 grid, depending on cage size.) (**c**) As in **b**, but with a 200-pN tip force. (**d**) Percentages of cages exhibiting the indicated maximum compressions during probing. Average maximum compressions for cage populations with maximum compressions <30 nm or >30 nM are shown (statistics in **Supplementary Table 2**). Source data for the graphs are available online.

at low Hsc70 concentrations by detaching Hsc70 from released triskelia, and Hsc70 then can cycle back to cages[38]. At 20 nM Hsc70, low Hsp110 levels enhanced disassembly, but higher levels resulted in less enhancement or modest inhibition together with a decrease in the initial scattering increase (**Fig. 6a**). With 250 nM Hsc70, increasing Hsp110 progressively decreased the initial scattering increase and slowed disassembly (**Fig. 6b**). Thus, when Hsc70 is limiting, Hsp110 accelerates disassembly by releasing Hsc70 from triskelia, but at higher Hsc70 concentrations, Hsp110 inhibits disassembly by also unloading Hsc70s from cages.

If decreasing the number of Hsc70s bound to cages decreases the forces driving disassembly, then self-association, by increasing the number of Hsc70s, should increase these forces. This possibility may explain why Hsc70 was more effective than Hsc70ΔC in disassembling +10-aa and +25-aa cages, whereas both disassembled 0-aa cages (**Fig. 2**), and why we observed gradual decreases in scattering with 0-aa cages in pH-6 reactions with Hsc70 (**Fig. 3a**) but not Hsc70ΔC (**Fig. 3g**), thus suggesting that only Hsc70 slowly disassembles these cages. To test this possibility, we used higher Hsc70ΔC and Hsc70 concentrations to increase self-association. When we reacted pH-6 cages with 5–42 μM Hsc70ΔC, scattering doubled (**Fig. 6c**), consistently with the scattering model's predictions (**Fig. 3i**) and data demonstrating that, at these concentrations, approximately two Hsc70ΔCs bind per CHC (**Fig. 5c**). With Hsc70, scattering increased but then dropped (**Fig. 6d**), thus revealing disassembly. EM of pH-6 cages reacted with excess Hsc70 or Hsc70ΔC confirmed that cages were disassembled by Hsc70 but not Hsc70ΔC, and that Hsc70 formed oligomers in such reactions, whereas Hsc70ΔC did not (**Supplementary Fig. 6**). Hsc70, but not Hsc70ΔC, therefore disassembles pH-6 cages, probably because of the greater self-association activity of Hsc70. The decreased disassembly by Hsc70ΔC compared with Hsc70 was not due to weaker binding, as shown by observations that Hsc70ΔC competed effectively with Hsc70 for binding to cages (**Supplementary Fig. 7**). The collision-pressure mechanism also predicts that increasing Hsc70 bulk can increase its disassembly activity. To test this possibility, we compared disassembly by histidine-tagged Hsc70 with or without anti-histidine Fab. Addition of Fab 1:1 with histidine-tagged Hsc70 accelerated disassembly (**Fig. 6e**) but had no effect on disassembly by untagged Hsc70 (**Fig. 6f**).

Hsc70 makes cages rigid but prone to catastrophic deformation

The collision-pressure model's predictions for Hsc70's effects on cage compressibility may be understood by analogy to balloons inflated to high versus low pressure. Just as gas-molecule collisions with a balloon's interior generate outwardly directed forces, bound Hsc70s may generate such forces on the interior walls of the cage. Cages with Hsc70s should therefore be less compressible than Hsc70-free cages when probed with a low force, just as high-pressure balloons are less compressible than low-pressure balloons (**Fig. 7a**). However, a high-pressure balloon is more prone to bursting—undergoing catastrophic deformation—when it is probed with a strong force, whereas a low-pressure balloon deforms rather than bursting (**Fig. 7a**). To test this possibility, we used AFM to measure the sizes and mean and maximum deformations of cages, cages with auxilin, and cages with auxilin and either Hsc70ΔC or Hsc70, at pH 6.0. In agreement with our cryo-EM data, the sizes of all of these were similar (**Supplementary Fig. 8**; **Supplementary Table 2**). With a 100-pN tip force, Hsc70 decreased the mean compressibility from 7.6 ± 0.16 to 6.3 ± 0.16 nm (**Fig. 7b**), but with a 200-pN force, Hsc70 increased the compressibility from 8.9 ± 0.18 to 11.9 ± 0.32 nm (**Fig. 7c**). Whereas the distribution of deformations was approximately Gaussian without Hsc70, the addition of Hsc70 led to a non-Gaussian distribution and appearance of a population of large (>15 nm) deformations (**Fig. 7c**), thus indicating that catastrophic deformation events were more frequent with Hsc70. To test this possibility, we measured the maximum deformation for each cage at a 100-pN force. Without Hsc70, 8% of cages exhibited maximum deformations of >30 nm, with a mean of 46 ± 2.5 nm, but with Hsc70, 30% of the cages exhibited deformations >30 nm, with a mean of 66 ± 1.5 nm (**Fig. 7d**). With the smaller

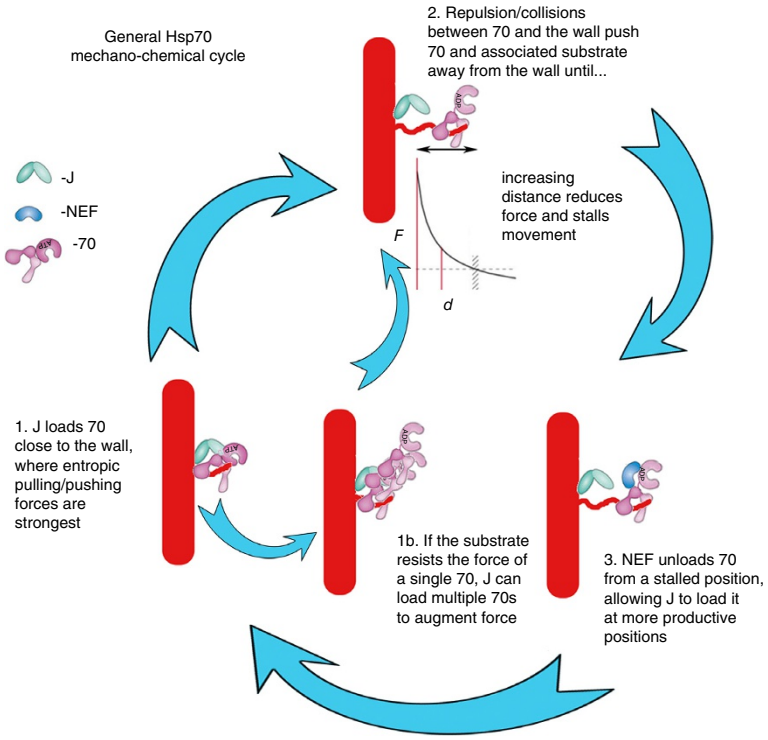

Figure 8 General model for the Hsp70 mechanochemical cycle. Step 1: J cochaperone loads Hsp70 (70) on substrate, close to a structural wall, where entropic pulling or pushing forces are strongest. Step 2: collisions and repulsion between Hsp70 and the wall push Hsp70 and the associated substrate away from the wall, but with increasing distance, the repulsive interactions, frequency of collisions and force diminish, so that movement stalls (the force (*F*) versus distance (*d*) exponential-decay curve is adapted from ref. 17). Step 3: a NEF unloads Hsp70 from the stalled position, thus allowing J to again load an Hsp70 close to the wall so that the cycle can continue. Step 1b: if the substrate does not yield to the force exerted by a single Hsp70, then the Hsp70 persists near the J cochaperone, thus allowing loading of additional Hsp70s onto the first and augmenting the force generated.

(<30 nm) deformations, Hsc70 had the opposite effect: the mean maximum deformations for this group were 15 ± 0.36 nm and 17 ± 0.33 nm with and without Hsc70, respectively. The effect of Hsc70 was therefore consistent with collision-pressure predictions: Hsc70 made cages less compressible when they were probed at low force but markedly increased the frequency of catastrophic deformations.

DISCUSSION

Support for a power stroke has rested, in part, on the conclusion that a Brownian ratchet cannot generate the force necessary to unfold the proteins that Hsp70s pull through translocation pores[12]. This conclusion was undermined by evidence that J proteins deposit Hsp70s on translocating substrates but then disengage, thus leaving the Hsp70 without a platform against which to push during the pulling[15,39]. Our observations that Fab binding at the same position as Hsc70 causes disassembly, and that Fab bound to Hsc70 enhances Hsc70's disassembly activity, further fail to support a power stroke and instead favor a mechanism in which the mass/volume ratio of a protein at this position causes disassembly. These results support either the collision-pressure or the Brownian/steric-wedge mechanism. However, the latter is not supported by the observation that disassembly persists even if Hsc70 is displaced by 25 aa, a distance that should relieve any direct steric clashes. By the process of elimination, collision pressure is the sole viable mechanism. But there is also evidence supporting this mechanism, which predicts that interposition of 10 or 25 residues between Hsp70 and a wall should slow disassembly ~10- and ~60-fold, respectively (**Supplementary Note 1**), in agreement with decreases observed with Hsc70ΔC or Fab. Our observation that Hsc70 makes cages more rigid but more likely to experience catastrophic deformations also supports this model. In addition, although our gel analyses and scattering data indicate that approximately two Hsc70ΔCs and multiple Hsc70s (per CHC) bind cages under conditions similar to those used for cryo-EM, the volume under the vertex attributable to the chaperones in the reconstructions accommodates only one or two PBDs for Hsc70ΔC or Hsc70, respectively. It is unlikely this scenario reflects most of the Hsc70s binding elsewhere on the cages, because binding of multiple Hsc70s requires an Hsc70-binding site in the CHC C termini (**Supplementary Fig. 5**). Density for most of the Hsc70s is therefore probably averaged out as a result of static or dynamic disorder, consistently with Hsc70s being mobile and able to exert collision pressure on cage walls.

The maximum calculated Hsp70 entropic pulling/pushing force of ~20 pN (refs. 16,17) may be compared with experimentally measured osmotic pressures of concentrated protein solutions, because osmotic pressure is the macroscopic product of microscopic collisions between proteins and membranes[31,32]: a 450 mg/ml solution of 67-kDa albumin generates 0.5 pN/nm^2 of osmotic pressure at pH 7.4 (ref. 40). If Hsc70 generates similar pressures, then an Hsc70 bound to the CHC tail under a cage vertex could generate a pushing force of ~20 pN (**Supplementary Note 1**). By comparison, the kinesin power stroke generates 5 pN (ref. 41) with a step size of 8 nm (ref. 42), whereas the force generated by an Hsp70 drops precipitously as it moves 1–2 nanometers away from a wall[16,17]. The work done by these systems is therefore similar, but the force mechanism is appropriately adapted to the function of each.

Whereas anti-FLAG Fabs disassemble FLAG-tag cages, they differ from Hsc70 in that they cannot actively cycle from released triskelia to cages. Auxilin loads Hsc70 on cages in preference to triskelia both because cages present a higher density and/or better positioning of binding sites for the multiple clathrin-binding motifs on the auxilin molecule[43] and because cage architecture places auxilin closer to Hsc70-binding sites[23,44]. Hsp110, the NEF in this system, stimulates disassembly when Hsc70 is limiting (**Fig. 6a**) by unloading Hsc70 from triskelia[38], but when Hsc70 is not limiting, high concentrations of Hsp110 inhibit disassembly by also unloading Hsc70 from cages (**Fig. 6b**). Similarly, Hsp70-mediated protein-disaggregation reactions are usually optimally stimulated by low Hsp110 concentrations[9,45,46], an observation that may be explained by invoking the role of geometry in the entropic pulling/pushing model. In this model, the role of the J cochaperone is not simply to load the Hsp70 onto substrate but to load it onto substrate at an optimal position: close to a wall, where entropic pulling/pushing forces are greatest (**Fig. 8**, step 1). Collisions and repulsion between the wall and Hsp70 push the two apart, but, as predicted by the entropic pulling/pushing

model and validated by our observations of the effects of shifting the Hsc70-binding sites in the clathrin cage, these pushing forces diminish with distance (**Fig. 8**, step 2). The reaction may stall if this distal Hsp70 sterically blocks loading of another Hsp70 at the more forcefully productive position, near the wall. The role of the NEF in the cycle is to unload the Hsp70 from the nonproductive position (step 3), but high NEF concentrations can be inhibitory if they also begin to unload Hsp70s from productive positions. In addition, if the substrate is recalcitrant and does not yield to the force of single Hsp70s (for example, clathrin cages at pH 6 versus pH 6.8), then the Hsp70 will remain close to the J cochaperone, thus allowing the latter to exploit the self-association properties of the chaperone to load additional Hsp70s onto the first and augment the forces (step 1b). Although this model does not suggest that Hsp110 cannot contribute to disaggregation via other mechanisms[47], it can account for the observed Hsp110 concentration dependence and can explain how the established functions of J cochaperones and NEFs in loading and unloading of substrates, respectively, in the Hsp70 chemical cycle, are harnessed in a mechanical cycle that generates the forces by which Hsp70s move and transform their substrates.

METHODS

Methods and any associated references are available in the online version of the paper.

Accession codes. Cryo-EM data have been deposited in the Electron Microscopy Data Bank under accession codes EMD-3442, EMD-4036 and EMD-4035 for clathrin cages, cages with Hsc70ΔC and cages with Hsc70, respectively.

Note: Any Supplementary Information and Source Data files are available in the online version of the paper.

ACKNOWLEDGMENTS

We thank L. Wang of UTHSCSA for technical assistance; T. Kirchhausen of HMS for CHC cDNA; C. Brantner and D. Sackett of NICHD, the NHLBI EM Core Facility for help with EM at an early stage of the work; and D. Sackett and R. Nossal at NICHD, D. Luque from ISCIII and J. Stachowiak from UT-Austin for helpful discussions. This work was supported by NS029051 (to E.M.L.) and GM118933 (to E.M.L. and R.S.); the NIH Intramural Research Program (NIBIB); and by grants BFU2013-44202 from the Spanish Ministry of Economy and Innovation and S2013/MIT-2807 from the Madrid Regional Government to J.M.V. H.-S.L. was supported in part by a scholarship from the Taiwan National Science Council (NSC103-2917-I-564-072).

AUTHOR CONTRIBUTIONS

R.S. designed and performed experiments, analyzed data and wrote the paper. H.-S.L., J.C., S.J., A.J.J. and E.M.L. designed and performed experiments, and analyzed data. J.M.V. designed experiments and analyzed data.

COMPETING FINANCIAL INTERESTS

The authors declare no competing financial interests.

1. Kim, Y.E., Hipp, M.S., Bracher, A., Hayer-Hartl, M. & Hartl, F.U. Molecular chaperone functions in protein folding and proteostasis. *Annu. Rev. Biochem.* **82**, 323–355 (2013).
2. Sousa, R. & Lafer, E.M. The role of molecular chaperones in clathrin mediated vesicular trafficking. *Front. Mol. Biosci.* **2**, 26 (2015).
3. Kityk, R., Kopp, J., Sinning, I. & Mayer, M.P. Structure and dynamics of the ATP-bound open conformation of Hsp70 chaperones. *Mol. Cell* **48**, 863–874 (2012).
4. Qi, R. *et al.* Allosteric opening of the polypeptide-binding site when an Hsp70 binds ATP. *Nat. Struct. Mol. Biol.* **20**, 900–907 (2013).
5. Zhuravleva, A., Clerico, E.M. & Gierasch, L.M. An interdomain energetic tug-of-war creates the allosterically active state in Hsp70 molecular chaperones. *Cell* **151**, 1296–1307 (2012).
6. Misselwitz, B., Staeck, O. & Rapoport, T.A. J proteins catalytically activate Hsp70 molecules to trap a wide range of peptide sequences. *Mol. Cell* **2**, 593–603 (1998).
7. Zuiderweg, E.R. *et al.* Allostery in the Hsp70 chaperone proteins. *Top. Curr. Chem.* **328**, 99–153 (2013).
8. Sousa, R.J. Structural mechanisms of chaperone mediated protein disaggregation. *Front. Mol. Biosci.* **1**, 12 (2014).
9. Rampelt, H. *et al.* Metazoan Hsp70 machines use Hsp110 to power protein disaggregation. *EMBO J.* **31**, 4221–4235 (2012).
10. Iosefson, O., Sharon, S., Goloubinoff, P. & Azem, A. Reactivation of protein aggregates by mortalin and Tid1: the human mitochondrial Hsp70 chaperone system. *Cell Stress Chaperones* **17**, 57–66 (2012).
11. Winkler, J., Tyedmers, J., Bukau, B. & Mogk, A. Chaperone networks in protein disaggregation and prion propagation. *J. Struct. Biol.* **179**, 152–160 (2012).
12. Voisine, C. *et al.* The protein import motor of mitochondria: unfolding and trapping of preproteins are distinct and separable functions of matrix Hsp70. *Cell* **97**, 565–574 (1999).
13. Matlack, K.E., Misselwitz, B., Plath, K. & Rapoport, T.A. BiP acts as a molecular ratchet during posttranslational transport of prepro-alpha factor across the ER membrane. *Cell* **97**, 553–564 (1999).
14. Misselwitz, B., Staeck, O., Matlack, K.E. & Rapoport, T.A. Interaction of BiP with the J-domain of the Sec63p component of the endoplasmic reticulum protein translocation complex. *J. Biol. Chem.* **274**, 20110–20115 (1999).
15. Sousa, R. & Lafer, E.M. Keep the traffic moving: mechanism of the Hsp70 motor. *Traffic* **7**, 1596–1603 (2006).
16. De Los Rios, P., Ben-Zvi, A., Slutsky, O., Azem, A. & Goloubinoff, P. Hsp70 chaperones accelerate protein translocation and the unfolding of stable protein aggregates by entropic pulling. *Proc. Natl. Acad. Sci. USA* **103**, 6166–6171 (2006).
17. Goloubinoff, P. & De Los Rios, P. The mechanism of Hsp70 chaperones: (entropic) pulling the models together. *Trends Biochem. Sci.* **32**, 372–380 (2007).
18. Ungewickell, E. *et al.* Role of auxilin in uncoating clathrin-coated vesicles. *Nature* **378**, 632–635 (1995).
19. Böcking, T., Aguet, F., Harrison, S.C. & Kirchhausen, T. Single-molecule analysis of a molecular disassemblase reveals the mechanism of Hsc70-driven clathrin uncoating. *Nat. Struct. Mol. Biol.* **18**, 295–301 (2011).
20. Böcking, T. *et al.* Key interactions for clathrin coat stability. *Structure* **22**, 819–829 (2014).
21. Rothnie, A., Clarke, A.R., Kuzmic, P., Cameron, A. & Smith, C.J. A sequential mechanism for clathrin cage disassembly by 70-kDa heat-shock cognate protein (Hsc70) and auxilin. *Proc. Natl. Acad. Sci. USA* **108**, 6927–6932 (2011).
22. Van Jaarsveld, P.P., Nandi, P.K., Lippoldt, R.E., Saroff, H. & Edelhoch, H. Polymerization of clathrin protomers into basket structures. *Biochemistry* **20**, 4129–4135 (1981).
23. Xing, Y. *et al.* Structure of clathrin coat with bound Hsc70 and auxilin: mechanism of Hsc70-facilitated disassembly. *EMBO J.* **29**, 655–665 (2010).
24. Jiang, J., Prasad, K., Lafer, E.M. & Sousa, R. Structural basis of interdomain communication in the Hsc70 chaperone. *Mol. Cell* **20**, 513–524 (2005).
25. Jiang, J. *et al.* Structure-function analysis of the auxilin J-domain reveals an extended Hsc70 interaction interface. *Biochemistry* **42**, 5748–5753 (2003).
26. Jiang, J. *et al.* Structural basis of J cochaperone binding and regulation of Hsp70. *Mol. Cell* **28**, 422–433 (2007).
27. Rapoport, I., Boll, W., Yu, A., Böcking, T. & Kirchhausen, T. A motif in the clathrin heavy chain required for the Hsc70/auxilin uncoating reaction. *Mol. Biol. Cell* **19**, 405–413 (2008).
28. Benaroudj, N., Batelier, G., Triniolles, F. & Ladjimi, M.M. Self-association of the molecular chaperone HSC70. *Biochemistry* **34**, 15282–15290 (1995).
29. Aprile, F.A. *et al.* Hsp70 oligomerization is mediated by an interaction between the interdomain linker and the substrate-binding domain. *PLoS One* **8**, e67961 (2013).
30. Preissler, S. *et al.* Physiological modulation of BiP activity by trans-protomer engagement of the interdomain linker. *eLife* **4**, e08961 (2015).
31. Kramer, E.M. & Myers, D.R. Osmosis is not driven by water dilution. *Trends Plant Sci.* **18**, 195–197 (2013).
32. Kramer, E.M. & Myers, D.R. Five popular misconceptions about osmosis. *Am. J. Phys.* **80**, 694–699 (2012).
33. Wilbanks, S.M., Chen, L., Tsuruta, H., Hodgson, K.O. & McKay, D.B. Solution small-angle X-ray scattering study of the molecular chaperone Hsc70 and its subfragments. *Biochemistry* **34**, 12095–12106 (1995).
34. Ha, J.H. & McKay, D.B. ATPase kinetics of recombinant bovine 70 kDa heat shock cognate protein and its amino-terminal ATPase domain. *Biochemistry* **33**, 14625–14635 (1994).
35. Northrup, S.H. & Erickson, H.P. Kinetics of protein-protein association explained by Brownian dynamics computer simulation. *Proc. Natl. Acad. Sci. USA* **89**, 3338–3342 (1992).
36. Zanten, J.H.V. & Monbouquette, H.G. Characterization of vesicles by classical light scattering. *J. Colloid Interface Sci.* **146**, 330–336 (1991).
37. Andréasson, C., Fiaux, J., Rampelt, H., Mayer, M.P. & Bukau, B. Hsp110 is a nucleotide-activated exchange factor for Hsp70. *J. Biol. Chem.* **283**, 8877–8884 (2008).
38. Schuermann, J.P. *et al.* Structure of the Hsp110:Hsc70 nucleotide exchange machine. *Mol. Cell* **31**, 232–243 (2008).

39. Liu, Q., D'Silva, P., Walter, W., Marszalek, J. & Craig, E.A. Regulated cycling of mitochondrial Hsp70 at the protein import channel. *Science* **300**, 139–141 (2003).
40. Vilker, V.L., Colton, C.K. & Smith, K.A. The osmotic-pressure of concentrated protein solutions: effect of concentration and pH in saline solutions of bovine serum-albumin. *J. Colloid Interface Sci.* **79**, 548–566 (1981).
41. Svoboda, K. & Block, S.M. Force and velocity measured for single kinesin molecules. *Cell* **77**, 773–784 (1994).
42. Coy, D.L., Wagenbach, M. & Howard, J. Kinesin takes one 8-nm step for each ATP that it hydrolyzes. *J. Biol. Chem.* **274**, 3667–3671 (1999).
43. Scheele, U., Kalthoff, C. & Ungewickell, E. Multiple interactions of auxilin 1 with clathrin and the AP-2 adaptor complex. *J. Biol. Chem.* **276**, 36131–36138 (2001).
44. Fotin, A. *et al.* Structure of an auxilin-bound clathrin coat and its implications for the mechanism of uncoating. *Nature* **432**, 649–653 (2004).
45. Ben-Zvi, A., De Los Rios, P., Dietler, G. & Goloubinoff, P. Active solubilization and refolding of stable protein aggregates by cooperative unfolding action of individual hsp70 chaperones. *J. Biol. Chem.* **279**, 37298–37303 (2004).
46. Gao, X. *et al.* Human Hsp70 disaggregase reverses Parkinson's-linked α-synuclein amyloid fibrils. *Mol. Cell* **59**, 781–793 (2015).
47. Mattoo, R.U., Sharma, S.K., Priya, S., Finka, A. & Goloubinoff, P. Hsp110 is a bona fide chaperone using ATP to unfold stable misfolded polypeptides and reciprocally collaborate with Hsp70 to solubilize protein aggregates. *J. Biol. Chem.* **288**, 21399–21411 (2013).
48. Zhu, X. *et al.* Structural analysis of substrate binding by the molecular chaperone DnaK. *Science* **272**, 1606–1614 (1996).

ONLINE METHODS

DNA constructs. DNA encoding rat clathrin heavy chain 1 (CHC) was PCR-amplified from DNA obtained from the Kirchhausen laboratory[19] with primer pair 1/2, and cloned into pET28a+ (Novagen). The +10-aa and +25-aa CHC DNAs were constructed by deleting nucleotides encoding the QLMLT sequence by using a QuikChange mutagenesis kit (Agilent Technologies). This was accomplished through amplification with primer pair 3/4, then re-addition of the QLMLT coding sequence 10 or 25 aa downstream by using primer pairs 5/6 and 7/8, respectively. CHC FLAG, +10-aa FLAG and +25-aa FLAG DNAs were constructed by replacing the sequence encoding QLMLT in CHC, CHC +10 aa and CHC +25 aa with a sequence encoding DYKDDDDK (FLAG tag), by using primer pairs 9/10, 11/12 and 13/14, respectively (primer sequences in **Supplementary Data Set 1**). DNA encoding clathrin light chain A1 (CLCA1) was amplified from pPPA1-2 rat LCA1 with primer pair 15/16 and cloned into pBAT4 (EMBL).

Protein expression and purification. BL21(DE3) cells (Agilent) with plasmid encoding histidine-tagged CHC were grown to an OD_{600} of 1.0 at 30 °C in 2× YT, transferred to 12 °C, induced with IPTG to 1 mM and incubated for 24 h. Cells from 1 L culture were pelleted and resuspended in 50 mL 0.5M Tris, pH 8.0, and 10 mM β-ME (lysis buffer) with one Roche protease-inhibitor-cocktail tablet. Cells were lysed by sonication and the addition of 2.5 mL 20% Triton X-100 and were centrifuged at 125,000*g* for 30 min. Supernatants were loaded onto 20 mL of Ni–NTA agarose (Qiagen), washed with 200 mL lysis buffer and eluted with 100 mL of 0.4 M Tris, pH 8.0, 10 mM β-ME and 200 mM imidazole. Protein was precipitated with an equal volume of saturated $(NH_4)_2SO_4$ and fractionated on a Superpose 6 (GE Healthcare) column in 0.5 M Tris, pH 7.0, 1 mM EDTA and 3 mM DTT (storage buffer). Pure proteins were concentrated by NH_4SO_4 precipitation, dialyzed into storage buffer, flash frozen in liquid N_2 and stored at −80 °C. CLCA1 was coexpressed with histidine-tagged CHC, because expression of CLCA1 alone led to its degradation, and was purified by Ni–NTA agarose as described above. Copurified proteins were incubated at 95 °C for 5 min to precipitate CHC, which was removed by centrifugation. Pure CHC and CLCA1 were mixed 1:1 for use in subsequent experiments. Hsc70 and auxilin(547–910) were prepared as previously described[38]. Anti-FLAG Fab was obtained by digestion of anti-FLAG M2 (Sigma; cat. no. F-1804; lot SLBG5673V) with a mouse IgG1 Fab preparation kit (Thermo). Validation of this monoclonal antibody is provided in ref. 49. For the experiments using anti-histidine Fab, clathrin was purified from clathrin-coated vesicles[24] from bovine brains obtained from a commercial slaughterhouse, auxilin(547–910) was prepared by thrombin cleavage of GST-auxilin(547–910)[25], and bovine Hsc70 with an N-terminal decahistidine tag was used so that Hsc70 would be the only histidine-tagged protein in the reaction. Anti-histidine Fab was obtained by digestion of anti-histidine monoclonal antibody (Miltenyi cat. no. 130-095-212; antibody GG11-8F3.5.1) with a mouse IgG1 Fab preparation kit (Thermo). Validation of this antibody is provided on the manufacturer's website.

Clathrin polymerization. CHC and CLCA1 were mixed 1:1 at 4.5 μM in storage buffer and dialyzed against 100 mM MES, pH 6.2, 1.5 mM $MgAc_2$ and 2 mM DTT (polymerization buffer) for 7 h, then dialyzed overnight against 20 mM imidazole, pH 6.8, 10 mM $(NH_4)_2SO_4$, 25 mM KCl, 2 mM $MgAc_2$ and 2 mM DTT, or 20 mM MES, pH 6.0, 10 mM $(NH_4)_2SO_4$, 25 mM KCl, 2 mM $MgCl_2$ and 2 mM DTT (DTT was omitted from all experiments with Fab). After dialysis, the sample was centrifuged at 9,000*g* for 10 min to remove aggregated material. EM of cages revealed that cages prepared from recombinant clathrin were indistinguishable from those prepared with clathrin purified from bovine brain clathrin-coated vesicles (data available upon request).

Stoichiometry of protein binding to cages. Cages polymerized as described above were dialyzed overnight against 20 mM MES, pH 6.0, 2 mM $MgCl_2$, 25 mM KPO_4 and 10 mM $(NH_4)_2SO_4$, diluted to 0.15 μM CHC and mixed with 0.23 μM histidine-Aux(547–910), 0.5 mM ATP and the indicated concentrations of Hsc70, Hsc70ΔC or anti-FLAG Fab. Reactions (200 μl) were centrifuged at 400,000*g* at 4 °C for 10 min to pellet cages and associated proteins. Pellets were suspended in 75 μl of 1× SDS sample buffer and resolved by denaturing PAGE. Proteins were imaged with a Bio-Rad Criterion Stain Free Imager and quantified with Bio-Rad Image Lab 2.0 software by comparison to lanes in which defined amounts of each protein were loaded. Experiments in which cages were omitted were run side by side to determine the background pelleting of each protein in the absence of cages. Uncropped images of gels in **Figure 5** are presented in **Supplementary Data Set 2**.

Stopped-flow experiments. Light-scattering experiments were carried out in an Applied Photosystems stopped-flow fluorometer with excitation/emission wavelengths of 395 nm. Cages corresponding to 0.3 μM CHC (unless otherwise indicated in figure legends) with 1 mM ATP and 0.45 μM auxilin in 20 mM imidazole, pH 6.8, 10 mM $(NH_4)_2SO_4$, 25 mM KCl and 2 mM $MgAc_2$ or 20 mM MES, pH 6.0, 10 mM $(NH_4)_2SO_4$, 25 mM KCl and 2 mM $MgCl_2$ were reacted with an equal volume of 0.04 μM to 8 μM Hsc70 in the same buffer. Background scattering determined from reactions without cages was subtracted from measured scattering values, which were normalized by dividing by the starting scattering value so that the initial scattering in all reactions was 1.0. Measures of scattering by varying concentrations of cages or triskelia showed that scattering was linear with cage or triskelia concentrations over the ranges used in these experiments (**Supplementary Fig. 1**). As indicated in the figure legends, auxilin and/or ATP were omitted from some reactions to control for the effects of these molecules. Removal of ATP (or substitution with ADP or ATP-γS), auxilin, the Hsc70 NBD, or Hsc70 ATP binding or hydrolysis activity severely slowed or abrogated disassembly (**Supplementary Fig. 1**).

Atomic force and electron microscopy. QNM peak-force AFM experiments were carried out on a multimode 8-nanoscope V instrument (Bruker) under pH-6.0 buffer, with an MSCT cantilever with a calibrated spring constant designed between 0.01 and 0.03 N/m and peak-force set points of 100–200 pN; 5-μl drops of fresh cages with or without auxilin, ATP, and Hsc70 or Hsc70ΔC were deposited on freshly peeled mica and imaged under the same buffer after routine optimization for biological AFM. Data were analyzed with instrument software (Nanoscope ver8.15, Bruker) and exported as ascii files for further analysis with Excel (Microsoft) and displayed with ImageJ (version 1.4x, NIH). Samples as described for AFM were absorbed for 20 s to a Formvar-carbon grid, rinsed and incubated 20 s with 1% uranyl acetate. Grids were wicked, air-dried and examined at 25,000× magnification in a JEOL JEM 1200EX-II.

Cryo-electron microscopy reconstructions. CHC and CLCA1 were mixed 1:1 at 4.5 μM in storage buffer, the clathrin-assembly domain of AP180 was added at 4.5 μM (GST-C58)[50], and the samples were dialyzed against 20 mM MES, pH 6.0, 10 mM $(NH_4)SO_4$, 25 mM KCl, 2 mM $MgCl_2$ and 2 mM DTT. After dialysis, the sample was centrifuged at 9,000*g* for 10 min to remove aggregates. Cages were then incubated with 1 mM ATP, auxilin (1.3:1 molar ratio to CHC) and either Hsc70ΔC or Hsc70 (at a 10:1 molar ratio to CHC), and aliquots of each sample were applied to glow-discharged holey carbon grids (Quantifoil R 1.2/R 1.3 300 mesh grids) containing an additional continuous thin layer of carbon, blotted and frozen in liquid ethane. Images were acquired under minimal dose conditions with an FEI Tecnai G2 FEG200 electron microscope at 200 kV with a Gatan side-entry cryo-holder at a nominal magnification of 41000× and underfocus values from 2 to 8 μm with a 16-megapixel FEI Eagle CCD camera with a step size of 15 um; thus, the pixel size of the acquired images was 3.65 Å (representative images of the cages are shown in **Supplementary Data Set 3**). The contrast transfer function of each image was estimated with CTFFIND3 (ref. 51). Single particles were manually selected and extracted with XMIPP3 (ref. 52). Particles were classified with a free-pattern maximum-likelihood method (Relion 2D-classification)[53]. To evaluate the structural homogeneity of the different data sets, Relion 3D classifications were performed[54], and the D6 particles were selected and used for the 3D reconstruction with projection matching from XMIPP[55]. A total of 3,468, 5,609 and 4,891 particles were used for the 3D reconstruction of cages, cages + Hsc70ΔC and cages + Hsc70, respectively. The resolutions obtained for the 3D reconstruction of the cages, cages + Hsc70ΔC and cages + Hsc70 were 28.5 Å, 28.5 Å and 28.7 Å, respectively[56]. For the subtraction maps, the volumes used were first normalized and filtered to the same resolution (30 Å), then scaled to approximately the same dimensions and finally subtracted with the 'vop subtract' option in the Chimera package[57]. The same procedure was used to subtract the clathrin D6 coat with Hsc70 and auxilin (EMD-5118 (ref. 23)) from the clathrin D6 coat (EMD-5119 (ref. 44)), as shown in **Figure 4a**,**d**. Chimera was also used for the visualization of the volumes and docking of the atomic structures.

doi:10.1038/nsmb.3272

Data fitting. We followed Rothnie *et al.*[21] and used Dynafit—which fits reaction schemes as sets of simultaneous differential equations—to fit our light-scattering data. In Dynafit scripts, a question mark after a parameter value indicates that the value is to be varied during fitting. The sequential aspect of the scheme used by Rothnie *et al.*[21] to globally fit their data is expressed by having three steps for Hsc70–ATP binding to cages and three steps for the transformation of Hsp70–ATP to Hsp70–ADP, corresponding to sequential loading of an Hsc70 onto each CHC in a triskelion. It also contains five global adjustable parameters (k_a and k_d, corresponding to the bimolecular association rate for Hsc70 binding to cages and the monomolecular rate of cage disassembly, respectively; k_r, corresponding to the rate of ATP hydrolysis; and scattering amplitudes for the starting (CA) and intermediate (CAT) species); and three locally adjustable parameters: an offset (the scattering value of the end state), and the concentrations of the clathrin cages (CA) and Hsc70 (T) for each data set with different Hsc70 concentrations (i.e., a total of 21 adjustable parameters for the example shown with data for six different Hsc70 concentrations: one cage and one Hsc70 concentration is fixed to anchor the fitting). We obtained good fits to our data with this script (Rothnie *et al.* fit, **Supplementary Note 2**), but it required cage and Hsc70 concentrations to vary as much as 2× from their experimentally input values and therefore seemed unreasonable. When concentrations were fixed as experimental inputs, the quality of the fits was poor, especially at lower Hsc70 concentrations. We therefore used a script (Simplefit, **Supplementary Note 2**) corresponding to the simplest scheme that could still capture our reaction profiles and fitted our averaged data individually at each Hsc70 concentration (all reactant concentrations were fixed as experimental inputs). It contains only three adjustable parameters (k_a and k_d, as defined above, and the amplitude of the scattering of the intermediate (CAT) species), and it was used simply to allow extraction of the global rate ($1/(1/k_a \times [\text{Hsc70}] + 1/k_d)$) of the reaction at different Hsc70 concentrations, because determination of this global rate was robust, but the three adjustable parameters were too tightly coupled (**Supplementary Fig. 2**) to allow for confident determinations of their values. Global disassembly rates at different Hsc70, Hsc70ΔC or Fab concentrations were then fitted with a Hill equation with the cooperativity parameter set to 1.0 to extract the maximal (V_{max}) disassembly rate and the Hsc70/Hsc70ΔC/Fab concentration at which rates were half-maximal, as described in Results. In cases in which velocities did not plateau at the concentrations tested (for example, with Hsc70ΔC and +10-aa or +25-aa cages in **Figure 2h**,**i**, we compared velocities at the highest (2 μM) Hsc70ΔC concentrations used). With Fab and 0-aa FLAG cages, disassembly appeared to be incomplete, so fitting was also carried out by fixing final scattering to correspond to complete disassembly (20% of starting intensity), thus resulting in the smaller V_{max} and $[\text{Fab}]_{1/2V\text{max}}$ values reported in **Figure 2j**. With Fab and +10-aa FLAG or +25-aa FLAG cages, the initial binding and subsequent disassembly phases were well separated, thus allowing the separate bimolecular association (k_a) and single-exponential-decay (disassembly) rates (k_u) to be individually fitted, as presented in **Figure 2k**,**l** (again, values were fitted by either allowing the final scattering intensity to vary or fixing it at 20% of the initial value, thus resulting in two values for each parameter).

Statistics. The minimal number of experimental repetitions was set so that the s.d. ranges for experimentally determined values (that were concluded to differ) were nonoverlapping, though in almost all cases the number of repeats (as specified in individual figure legends or **Supplementary Table 3**) exceeded the minimal number by several fold. A small number (<5%) of data from experimental replicates were excluded when the experimental outcome (for example, value of a rate determination) differed by >2.5 s.d. from the mean of experiments carried out under ostensibly identical conditions and when a reason for the variation (for example, bubbles in the stopped-flow apparatus or the aging of labile reagents) was clear.

49. Brizzard, B.L., Chubet, R.G. & Vizard, D.L. Immunoaffinity purification of FLAG epitope-tagged bacterial alkaline phosphatase using a novel monoclonal antibody and peptide elution. *Biotechniques* **16**, 730–735 (1994).
50. Ye, W. & Lafer, E.M. Clathrin binding and assembly activities of expressed domains of the synapse-specific clathrin assembly protein AP-3. *J. Biol. Chem.* **270**, 10933–10939 (1995).
51. Mindell, J.A. & Grigorieff, N. Accurate determination of local defocus and specimen tilt in electron microscopy. *J. Struct. Biol.* **142**, 334–347 (2003).
52. Abrishami, V. *et al.* A pattern matching approach to the automatic selection of particles from low-contrast electron micrographs. *Bioinformatics* **29**, 2460–2468 (2013).
53. Scheres, S.H. RELION: implementation of a Bayesian approach to cryo-EM structure determination. *J. Struct. Biol.* **180**, 519–530 (2012).
54. Scheres, S.H. & Chen, S. Prevention of overfitting in cryo-EM structure determination. *Nat. Methods* **9**, 853–854 (2012).
55. de la Rosa-Trevín, J.M. *et al.* Xmipp 3.0: an improved software suite for image processing in electron microscopy. *J. Struct. Biol.* **184**, 321–328 (2013).
56. Penczek, P.A. Three-dimensional spectral signal-to-noise ratio for a class of reconstruction algorithms. *J. Struct. Biol.* **138**, 34–46 (2002).
57. Pettersen, E.F. *et al.* UCSF Chimera: a visualization system for exploratory research and analysis. *J. Comput. Chem.* **25**, 1605–1612 (2004).